NACA

RESEARCH MEMORANDUM

FLIGHT INVESTIGATION OF ENGINE NACELLES AND WING VERTICAL POSITION ON THE DRAG OF A DELTA-WING AIRPLANE CONFIGURATION FROM MACH NUMBER 0.8 TO 2.0

By Joseph H. Judd

Langley Aeronautical Laboratory
Langley Field, Va.

NATIONAL ADVISORY COMMITTEE
FOR AERONAUTICS

WASHINGTON
March 9, 1954

Classification cancelled (or changed to) UNCLASSIFIED

By Authority of NASA TECH PUB. ANNOUNCEMENT #121
(OFFICER AUTHORIZED TO CHANGE)

By 4 Nov 57
NAME AND

GRADE OF OFFICER MAKING CHANGE)

26 Mar 61
DATE

NATIONAL ADVISORY COMMITTEE FOR AERONAUTICS

RESEARCH MEMORANDUM

FLIGHT INVESTIGATION OF ENGINE NACELLES AND WING VERTICAL POSITION ON THE DRAG OF A DELTA-WING AIRPLANE CONFIGURATION FROM MACH NUMBER 0.8 TO 2.0

By Joseph H. Judd

SUMMARY

Flight tests were made of a 60° delta wing (NACA 65A003 airfoil section) mounted in midwing and high-wing positions on a modified transonic body from Mach numbers 0.8 to 2.0 and Reynolds numbers based on wing mean aerodynamic chord, from 5.8×10^6 to 22.8×10^6. Ducted nacelles, with external contours similar to ram-jet nacelles, were mounted at 66 percent of the wing semispan symmetrically on the midwing configuration and under the wings on the high-wing configuration.

Over the Mach number range tested, the high-wing configuration without nacelles had higher drag coefficients than the midwing configuration without nacelles, although both configurations had approximately the same longitudinal area distribution and frontal area. Thus, secondary interference effects caused by wing-body root interference brought about appreciable effects in drag coefficients. The same order of drag increase was observed at supersonic speeds for the configurations with nacelles.

INTRODUCTION

The Langley Pilotless Aircraft Research Division has tested rocket-powered models of wing-fuselage-nacelle combinations as part of a general aerodynamic investigation of nacelles and stores. Some examples of the effects of nacelle location on the drag of sweptback-wing—fuselage configurations have been reported in references 1 and 2. However, much of the previous work on delta-wing configurations has dealt with the installation of stores and armament packets, for example, reference 3. The tests reported herein were made to show the effect of engine nacelles and wing vertical location on the drag of a delta-wing airplane configuration.

[redacted]

[redacted]

A considerable amount of effort has been expended to determine low-drag wing-fuselage combinations for use on supersonic airplane configurations. References 4 and 5 summarize test results for a wide range of wing plan forms on various bodies of revolution. After a study of these results, a 60° delta wing (NACA 65A003 airfoil sections) was chosen because of its low supersonic drag and structural feasibility for application to interceptor planes. To make the tests realistic insofar as component sizes were concerned, the design of a supersonic ram-jet interceptor (design Mach number 2.0) was outlined. The original estimates of coefficients are tabulated as follows:

Zero-lift drag coefficient, C_{D_0}	0.0166
Induced drag factor, $C_D/C_L{}^2$	0.433
Lift coefficient, C_L	0.1072
Gross thrust coefficient, $C_{T_{gross}}$	1.0

The engines located in nacelles on the wings were of sufficient size to maintain a 2.8g turn at 60,000 feet without losing speed.

In order to obtain higher Mach numbers, the afterbody of the airplane configuration was cut off so that a sustainer rocket motor could be inserted into the fuselage. The test models then consisted of a 60° delta wing mounted on a modified transonic body (ref. 1). Nacelles having the external contour of a ram-jet engine nacelle were located at 66 percent of the wing semispan.

All tests reported herein were conducted at the Langley Pilotless Aircraft Research Station at Wallops Island, Va. Rocket-powered models of the airplane configurations were flown and a half-size nacelle was shot from a helium gun. The Reynolds number range, based on wing mean aerodynamic chord, of the flight tests was from 5.8×10^6 to 22.8×10^6 and the Mach number range was from 0.8 to 2.0. In addition, the internal nacelle drag was determined from free-jet tests in the preflight jet.

SYMBOLS

A	cross-sectional area, normal to fuselage center line, sq in.
C_D	drag coefficient, based on wing area
C_{D_N}	nacelle drag coefficient, two nacelles based on wing area
C_{D_0}	zero-lift drag coefficient, based on wing area
C_L	lift coefficient, based on wing area

C_N	normal-force coefficient, based on wing area
C_{p_b}	base pressure coefficient
$C_{T_{gross}}$	gross thrust coefficient, based on nacelle frontal area
d	diameter, in
l	fuselage length, in
M	Mach number
R	Reynolds number based on wing mean aerodynamic chord
r	radial distance from center line, in.
x	axial distance from fuselage nose, in.
y	distance normal to nacelle axis, in.

MODELS

Figures 1 and 2 present three-view drawings and photographs of the rocket-powered flight models. Four models were tested, a midwing configuration, a midwing configuration with symmetrical nacelles, a high-wing configuration, and a high-wing configuration with underslung nacelles. The midwing models had the wing mean chord plane passing through the fuselage center line and the high-wing models had the wing mean chord plane located 0.115 wing semispans above the fuselage center line. In an attempt to place the nacelles as close to the center of gravity as possible, symmetrically mounted nacelles were used on the midwing configuration and underslung nacelles were mounted on the high-wing configuration. The center lines of the underslung nacelles were located 0.54 nacelle diameters below the wing chord plane and 0.04 diameters below the fuselage center line. The nacelles on both configurations were located at 66 percent of the wing semispan.

The basic geometric parameters for these models are given in table I. The variation of model cross-sectional area normal to model center line is plotted in figure 3 against axial distance. Also included in figure 3 are drawings of bodies of revolution the cross-sectional-area distributions of which are equivalent to those of the test models. Table II presents the location of the model center of gravity for each flight model.

The basic configuration consisted of a 60° delta wing (NACA 65A003 airfoil section parallel to free-stream direction) mounted on a modified

[redacted]

transonic body. Fuselage and airfoil ordinates are given in tables III and IV. Two aluminum fins of hexagonal airfoil section were located at the rear of the fuselage in the vertical plane. The fuselage was constructed of mahogany with a spun aluminum and Fiberglas nose for the telemeter fairing. A static pressure orifice was located at the base of the fuselage, midway between the rocket motor and the outer fuselage surface in a plane inclined 45° to the wing plane. The wing was constructed of laminated spruce over a 24S-T aluminum core and had steel inlays at the wing surface for added stiffness.

The ram-jet nacelles employed in these configurations have no afterbody convergence as is customary for turbojet nacelles. The nacelle forebody shape was a truncated cone and the rearward section was cylindrical. In order to obtain a high mass flow ratio and to keep internal drag low, a straight sharp-lipped duct was used for air flow through the nacelle. A sketch of the basic nacelle is presented in figure 4(a). At the base of the nacelle, eight pressure orifices were manifolded to give the average nacelle base pressure. The nacelles were constructed with Paraplex impregnated Fiberglas shells over balsa filler. In the midwing configuration the nacelle was built as part of the wing structure. The nacelles of the high-wing model were carried underneath the wings. In order to prevent a gap between the conical nacelle forebody and the wing leading edge, a smooth straight fairing was incorporated from the nacelle nose to the wing. The lines of the fairing between the nacelle and the wing are shown in the photograph presented as figure 5.

In order to determine the drag of the isolated nacelle at transonic speeds, an approximately half-scale model of the nacelle was constructed. Figures 4(b) and 6 present a sketch and photograph of the test nacelle. Three hexagonal airfoil fins were located at the rear of the nacelle to stabilize the model. The nose section was machined from brass and the rearward section of the model was constructed of mahogany and covered with Paraplex impregnated Fiberglas.

A duplicate of a model nacelle was constructed to determine the internal drag from free-jet tests. A photograph of the nacelle, mounted for testing, is shown as figure 7. The nacelle consisted of a steel tube with a mahogany fairing over the outer surface to form the nacelle contour. Three total-pressure tubes were located in a rake at the nacelle duct exit at $\frac{y}{r} = 0$, 0.84, and 0.97. A static-pressure orifice was located at the duct exit 45° from the plane of the rake.

TESTS AND INSTRUMENTATION

Flight Tests of Rocket-Propelled Models

The rocket-propelled models were launched from a mobile launcher. Figure 2(e) shows a midwing model with nacelles and its booster on the launcher prior to flight. A single ABL Deacon rocket motor propelled the combination to supersonic speeds. After separation of the test model from the booster, a 3.25-inch aircraft rocket in the fuselage of the model accelerated the configuration to the peak Mach number. The information presented in this report was obtained during the decelerating flight after sustainer-rocket burnout. The range of Reynolds number, based on the wing mean aerodynamic chord, and Mach number obtained during flight tests of the configuration is presented in figure 8.

Data for the flight tests were obtained by use of a telemeter, a CW Doppler velocimeter, tracking radar, tracking cameras, and radiosonde. The radiosonde, borne aloft by a balloon, gives a survey of the atmospheric conditions over the altitude range covered by the models. In addition, the radiosonde balloon was tracked by the radar to determine the velocity and direction of the winds aloft. The drag coefficient of the models was obtained by differentiation of the model velocity and use of atmospheric data from the radiosonde. All model velocities were corrected for wind velocity prior to these computations.

Each of the rocket-propelled models carried a nose telemeter unit to transmit flight data to ground-receiving stations. The midwing configuration had a two-channel unit for transmitting fuselage base pressure and longitudinal acceleration. The other models employed four-channel telemeters. The high-wing configuration transmitted normal and longitudinal acceleration, total pressure, and fuselage base pressure. The midwing configuration with nacelles had channels for fuselage and nacelle base pressure, total pressure, and longitudinal acceleration, whereas, the high-wing configuration with nacelles had channels for fuselage and nacelle base pressure, total pressure, and normal acceleration. The Mach number obtained from total pressure measurements was used as a correlation of the wind-corrected Mach number obtained from the CW Doppler velocimeter. Drag coefficients were obtained from longitudinal accelerometer data and, together with the CW Doppler drag data, were used to obtain the drag-coefficient curves presented herein. The base pressure coefficients and base drag coefficients were determined from the base pressure measurements.

Helium-Gun Tests of Nacelle

A half-scale finned model of the nacelle was placed in a balsa cradle and fired from the helium gun. After leaving the muzzle, the cradle split

and the nacelle flew a ballistic trajectory. Data for this flight test were obtained from a CW Doppler velocimeter, tracking radar, and radiosonde. The model drag coefficient was computed by differentiation of the model velocity and use of atmospheric data from the radiosonde. The Reynolds number, based on the wing mean aerodynamic chord, and Mach number range for this test are presented in figure 8.

Free-Jet Tests of Nacelle

In order to determine the supersonic losses of the nacelle duct, tests of the nacelle were made in a free-jet at Mach numbers of 1.2, 1.4, and 1.8. The nacelle inlet was placed near the nozzle so expansion or compression waves caused by over or under expansion of the nozzle would fall behind the nacelle lip. In addition to the total and static pressures at the nacelle exit, the nozzle total and static pressures and the jet stagnation temperatures were measured. Inasmuch as the nacelle axis was alined with the jet center line, the flow at the nacelle exit was assumed to be symmetrical. In addition, the static pressure across the jet was assumed to be constant. Then the nacelle internal drag was computed by the use of momentum relationships.

Test Accuracy

The basic accuracy of drag coefficients has been established in reference 1 by comparison of the drag coefficients from three similar models. The errors found include those due to model dissimilarities caused by construction and finish and those due to the instrumentation error of the CW Doppler velocimeter, tracking radar, and radiosonde. On the basis of statistical data compiled by the Instrument Research Division of the Langley Laboratory, it is believed that the probable error is within ±1 percent of the full-scale range for the telemeter instruments. Thus, the probable error is within the values tabulated as follows:

M	ΔM	Fuselage ΔC_{p_b}	Nacelle ΔC_{p_b}	Fuselage base ΔC_D	Nacelle base ΔC_D	ΔC_{D_N} (internal)	Measured ΔC_D
0.9	±0.005	±0.016	±0.026	±0.0005	±0.0010	±0.0001	±0.0007
1.1	±.005	±.012	±.019	±.0003	±.0007	±.0001	±.0007
1.6	±.005	±.006	±.008	±.0002	±.0003	±.0001	±.0007

These values were used to compute the total error in the drag coefficients of the various test models and indicate the measure of validity attached

[redacted]

to comparisons made between configurations. The total errors are tabulated as follows:

M	ΔC_D (without nacelles)	ΔC_D (with nacelles)	ΔC_{D_N} (external)
0.9	±0.0007	±0.0018	±0.0025
1.1	±.0007	±.0015	±.0022
1.6	±.0007	±.0011	±.0018

The accuracy of measurements made on models propelled from the helium gun has been determined by experience obtained from previous tests. The Mach number error is within ±0.005 and the error in drag coefficient is within ±0.0008.

RESULTS AND DISCUSSION

Nacelle Internal Drag

The supersonic internal drag of the straight duct was obtained from the free-jet tests just described. Shadowgraphs of the flow at the nacelle inlet are shown in figure 9. The shock wave attaches to the nacelle lip at Mach number 1.25 and the flow becomes supersonic in the duct. The internal drag was obtained from momentum relationships in the duct and is presented in figure 10. This internal drag coefficient is for two nacelles and is based on the total wing area of the models. The internal drag of a straight-duct nacelle at subsonic and transonic speeds has been determined from wind-tunnel tests and is given in reference 6. These values of internal drag coefficient, when referred to the wing areas of the present tests, varied between 0.0011 and 0.0009 which correlates with the supersonic data presented herein.

Configuration Drag

Figure 11 presents the total drag coefficient (based on wing area) for two nacelles obtained from helium-gun tests of the isolated nacelle. The fin drag coefficient obtained from unpublished data has been subtracted. Figures 12, 13, 14, and 15 give the basic test data for the midwing configuration, the midwing configuration with symmetrical nacelles, the high-wing configuration, and the high-wing configuration with underslung nacelles. The fuselage base pressure coefficients, fuselage base drag coefficients, and the total drag coefficients are presented for the

midwing and high-wing models without nacelles. In addition, nacelle base pressure coefficients and base drag coefficients are given for the models with nacelles.

The drag coefficients of the high-wing and midwing configurations without nacelles are compared in figure 16. The high-wing configuration had a higher drag coefficient over the Mach number range of these tests and had a slightly lower force break Mach number than the midwing configuration. An inspection of the base drag coefficients for these models over the Mach number range for which data are available indicated that the difference in base drag coefficients was approximately the same as the difference in model drag coefficients. However, the difference in base drags indicates an additional wing-body interference over the model base and wake. An inspection of the area distributions of the models (fig. 3) was made to determine whether the difference in drag coefficients could be explained according to the transonic area rule (ref. 7). Both models have similar longitudinal area distributions and the same length. Thus, the transonic drag-rise increment might be expected to be proportional to the ratio of maximum cross-sectional areas. However, the frontal area ratio was 1.058, whereas, the ratio of the drag rise increments was 1.383. In an effort to localize the region which could appreciably affect the pressure drag, the afterbodies of the equivalent bodies of revolution of the configuration were compared with those of reference 8. The effect of the afterbody length-to-diameter ratio and the ratio of base area to maximum area was considered. The ratio of base pressure drag plus afterbody pressure drag at Mach number 1.2 for the afterbodies of the midwing and high-wing configurations (estimated from data in ref. 8) was only 1.044 which was considerably below that of the test configurations. Thus, it appears that the wing-fuselage juncture affects the interference drag to a large extent.

A comparison of the external drag coefficients for the midwing and high-wing configurations with nacelles is presented in figure 17. In order to obtain the external drag coefficients, the nacelle internal and the base pressure coefficients were subtracted from the total drag coefficients. The drag coefficients of the high-wing configuration were larger than those of the midwing configuration over the entire Mach number range tested with the greatest difference occurring at Mach number 1.03. Below Mach number 0.97 the drag differences were small; whereas, at supersonic speeds the differences varied from 28 to 14 percent which was about the same as those of the configurations without nacelles. The transonic drag-rise increments up to Mach number 1.05 were 0.0051 and 0.0110 for the midwing and high-wing configurations with nacelles, respectively. A comparison of the fuselage base drag coefficients for the high-wing and midwing configurations shows that the difference in base drag coefficients is less than the difference in model drag coefficients over the test Mach number range. The midwing and high-wing configurations with nacelles have similar longitudinal cross-sectional area distributions

and the same length. Although the transonic drag rise would be expected to be proportional to the maximum cross-sectional area, the ratio of maximum cross-sectional area is 1.09, whereas the transonic drag rise ratio is 2.16.

The transonic area rule (ref. 7) states that slender wing-body combinations have the same zero-lift transonic drag rise as their equivalent bodies of revolution. However, information presented in reference 9 for several airplane configurations and in reference 10 for nacelle installations indicates that appreciable errors can result from this method of estimating the transonic drag rise. The data from the tests of midwing and high-wing configurations with and without nacelles suggest that local interference effects such as occur in the wing-fuselage juncture form part of the source of the discrepancy.

Nacelle Drag Coefficient

The variation of the nacelle plus interference drag coefficient is presented in figure 18. The drag coefficients of the symmetrical and underslung nacelles were obtained by subtracting the drag coefficients of the models without nacelles from that of the models with nacelles. The two-dimensional base drag coefficient was estimated from references 11 and 12 and subtracted from the isolated-nacelle flight-test data. These estimated nacelle base drag coefficients were compared with the measured values from the rocket-model nacelles and found to be of the right order of magnitude. In addition, the internal drag coefficient was subtracted from the isolated nacelle drag coefficient obtained from helium-gun tests. This procedure gave the external drag coefficient for the isolated nacelle to Mach number 1.15. The supersonic pressure drag was computed by the method of characteristics and values of skin friction drag (estimated from ref. 13) were added to give the isolated nacelle external drag coefficient to Mach number 1.8.

The drag coefficients for both symmetrical and underslung nacelles were larger than those of the isolated nacelle at transonic speeds. Above Mach number 1.1, the drag coefficients of both nacelles dropped below those of the isolated nacelle and then rose to about the same value as that of the isolated nacelle above Mach number 1.5. The symmetrical and underslung nacelle drag coefficients seemed to be approximately the same except for local effects.

Normal-Force Coefficient

In reference 14 the normal-force coefficients for symmetrical wing-body combinations are shown to be very small. The high-wing configurations, however, were asymmetrical models so the normal-force coefficients

were measured. The trim normal-force coefficients are presented in figure 19 for the high-wing configurations with and without nacelles. From the small magnitude of these coefficients, it can be seen that the drag due to lift was small and justifiably was neglected in the preceding drag comparisons.

For configurations composed of slender components, the pressure fields are small in amplitude and the main factor causing the model to trim is the displacement of the drags from the center of gravity of the model. When the supersonic drag coefficients remain nearly constant, a constant normal-force coefficient for trim is expected. The high-wing configuration without nacelles displayed this characteristic. The addition of nacelles to the high-wing configuration caused relatively large changes in trim normal-force coefficients over the Mach number range of these tests. Inasmuch as the center of gravity of the configuration remained approximately the same as that of the model without nacelles, the variation could have been caused by a forward shift of the center of pressure due to the nacelles. Another cause of the change could have been the additional interference of the nacelle on the wing. Because of the limitation in model instrumentation, the magnitude of each effect could not be determined.

CONCLUSIONS

Rocket-powered flight tests from Mach number 0.8 to 2.0 were made for a 60° delta wing (NACA 65A003 airfoil section) mounted on a modified transonic body in midwing and high-wing locations. Tests were made of models with nacelles mounted at 66 percent of the wing semispan with nacelle axes in the plane of the fuselage axis. The Reynolds numbers, based on wing mean aerodynamic chord, varied from 5.8×10^6 to 22.8×10^6. The following statements summarize the results of the tests:

(1) The drag coefficients for the high-wing configuration without nacelles were at least 19 percent greater than those of the midwing configuration without nacelles over the test Mach number range.

(2) At supersonic speeds the high-wing configuration with underslung nacelles had drag coefficients from 14 to 28 percent greater than the midwing configuration with symmetrical nacelles.

(3) The drag coefficients of both symmetrical and underslung nacelles were greater than those of the isolated nacelle up to Mach number 1.07.

Both nacelles had appreciable decreases in drag coefficients from Mach number 1.07 to 1.5, a condition which indicates favorable fuselage-nacelle interference.

Langley Aeronautical Laboratory,
National Advisory Committee for Aeronautics,
Langley Field, Va., December 3, 1953.

REFERENCES

1. Pepper, William B., Jr., and Hoffman, Sherwood: Comparison of Zero-Lift Drags Determined by Flight Tests at Transonic Speeds of Symmetrically Mounted Nacelles in Various Spanwise Positions on a 45° Sweptback Wing and Body Combination. NACA RM L51D06, 1951.

2. Hoffman, Sherwood, and Pepper, William B., Jr.: The Effect of Nacelle Combinations and Size on the Zero-Lift Drag of a 45° Sweptback Wing and Body Configuration as Determined by Free-Flight Tests at Mach Numbers Between 0.8 and 1.3. NACA RM L53E25, 1953.

3. Jacobsen, Carl R.: Effects of Size of External Stores on the Aerodynamic Characteristics of an Unswept and a 45° Sweptback Wing of Aspect Ratio 4 and a 60° Delta Wing at Mach Numbers of 1.41, 1.62, and 1.96. NACA RM L52K20a, 1953.

4. Morrow, John D., and Nelson, Robert L.: Large-Scale Flight Measurements of Zero-Lift Drag of 10 Wing-Body Configurations at Mach Numbers From 0.8 to 1.6. NACA RM L53D18a, 1953.

5. Hall, Charles F.: Lift, Drag, and Pitching Moment of Low-Aspect-Ratio Wings at Subsonic and Supersonic Speeds. NACA RM A53A30, 1953.

6. Bielat, Ralph P., and Harrison, Daniel E.: A Transonic Wind-Tunnel Investigation of the Effects of Nacelle Shape and Position on the Aerodynamic Characteristics of Two 47° Sweptback Wing-Body Configurations. NACA RM L52G02, 1952.

7. Whitcomb, Richard T.: A Study of the Zero-Lift Drag-Rise Characteristics of Wing-Body Combinations Near the Speed of Sound. NACA RM L52H08, 1952.

8. Stoney, William E., Jr.: Some Experimental Effects of Afterbody Shape on the Zero-Lift Drag of Bodies for Mach Numbers Between 0.8 and 1.3. NACA RM L53I01, 1953.

9. Hall, James Rudyard: Comparison of Free-Flight Measurements of the Zero-Lift Drag Rise of Six Airplane Configurations and Their Equivalent Bodies of Revolution at Transonic Speeds. NACA RM L53J21a, 1953.

10. Smith, Norman F., Bielat, Ralph P., and Guy, Lawrence D.: Drag of External Stores and Nacelles at Transonic and Supersonic Speeds. NACA RM L53I23b, 1953.

11. Chapman, Dean R., Wimbrow, William R., and Kester, Robert H.: Experimental Investigation of Base Pressure on Blunt-Trailing-Edge Wings at Supersonic Velocities. NACA Rep. 1109, 1952. (Supersedes NACA TN 2611.)

12. Morrow, John D., and Katz, Ellis: Flight Investigation at Mach Numbers From 0.6 to 1.7 To Determine Drag and Base Pressures on a Blunt-Trailing-Edge Airfoil and Drag of Diamond and Circular-Arc Airfoils at Zero Lift. NACA RM L50E19a, 1950.

13. Van Driest, E. R.: Turbulent Boundary Layer for Compressible Fluids on an Insulated Flat Plate. Rep. No. AL-958, North American Aviation, Inc., Sept. 15, 1949.

14. Schult, Eugene D.: Comparison of Large-Scale Flight Measurements of Zero-Lift Drag at Mach Numbers From 0.9 to 1.7 of Two Wing-Body Combinations Having Similar 60° Triangular Wings With NACA 65A003 Sections. NACA RM L50I22, 1950.

TABLE I

ROCKET-MODEL CHARACTERISTICS

Fuselage:	
Fineness ratio	10.0
Frontal area, sq ft	0.242
Wing:	
Aspect ratio	2.31
Taper ratio	0
Mean aerodynamic chord, ft	1.80
Airfoil	65A003
Total plan-form area, sq ft	4.21
Nacelle:	
Fineness ratio	4.94
Frontal area, sq ft	0.101
Inlet area, sq ft	0.0376
Fin:	
Aspect ratio	2.22
Area, sq ft	1.25
Area Ratios:	
Fuselage frontal area/wing area	0.0575
Fuselage base area/wing area	0.0286
Nacelle frontal area/wing area (2 nacelles)	0.0480
Nacelle annular base area/wing area (2 nacelles)	0.0300

TABLE II

LOCATION OF CENTER OF GRAVITY OF MODELS

Model	Center of gravity x, in.
Midwing	40.50
Midwing with nacelles	42.12
High wing	42.87
High wing with nacelles	42.12

TABLE III

FUSELAGE ORDINATES

Axial distance measured from nose, in.	Radius, in.
0	0
.4	.185
.6	.235
1.0	.342
2.0	.578
4.0	.964
6.0	1.290
8.0	1.577
12.0	2.074
16.0	2.472
20.0	2.772
24.0	2.993
28.0	3.146
32.0	3.250
36.0	3.314
40.0	3.334
44.0	3.304
48.0	3.219
52.0	3.037
56.0	2.849
60.0	2.661
64.0	2.474
66.7	2.347

TABLE IV

AIRFOIL ORDINATES AT THE MEAN AERODYNAMIC CHORD

Chordwise distance from the leading edge, in.	Vertical displacement from mean chord line, in.
0	0
.108	.050
.162	.061
.270	.077
.540	.106
1.080	.142
1.620	.172
2.160	.193
3.240	.236
4.320	.267
5.400	.290
6.480	.306
7.560	.318
8.640	.323
9.710	.323
10.800	.316
11.880	.301
12.970	.280
14.040	.255
15.120	.226
16.200	.192
17.280	.155
18.490	.117
19.400	.079
20.500	.046
21.600	.007

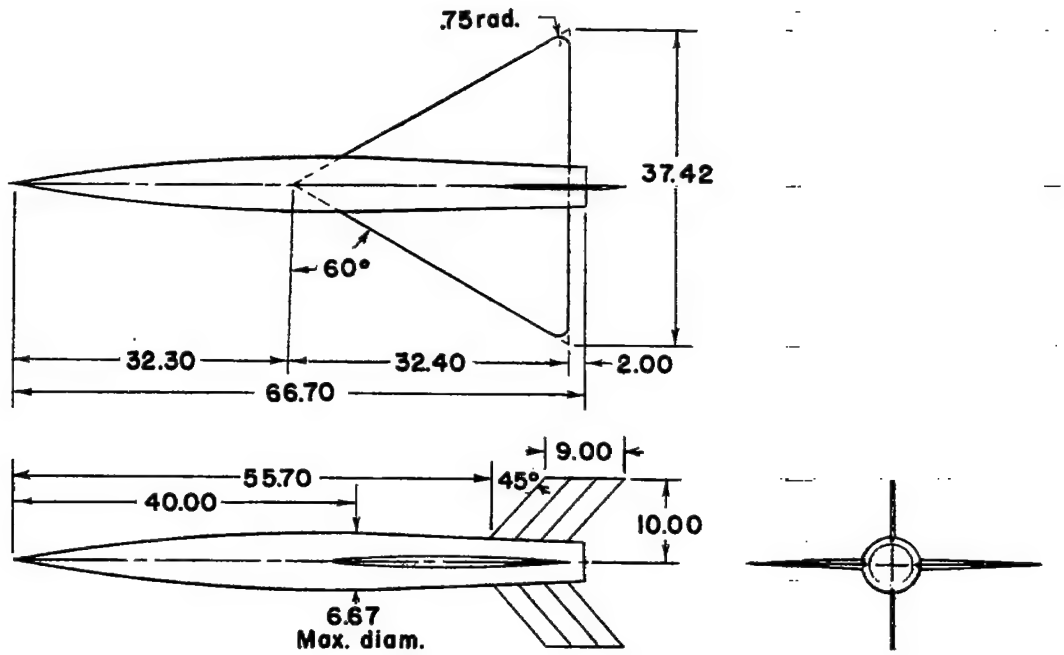

(a) Midwing configuration.

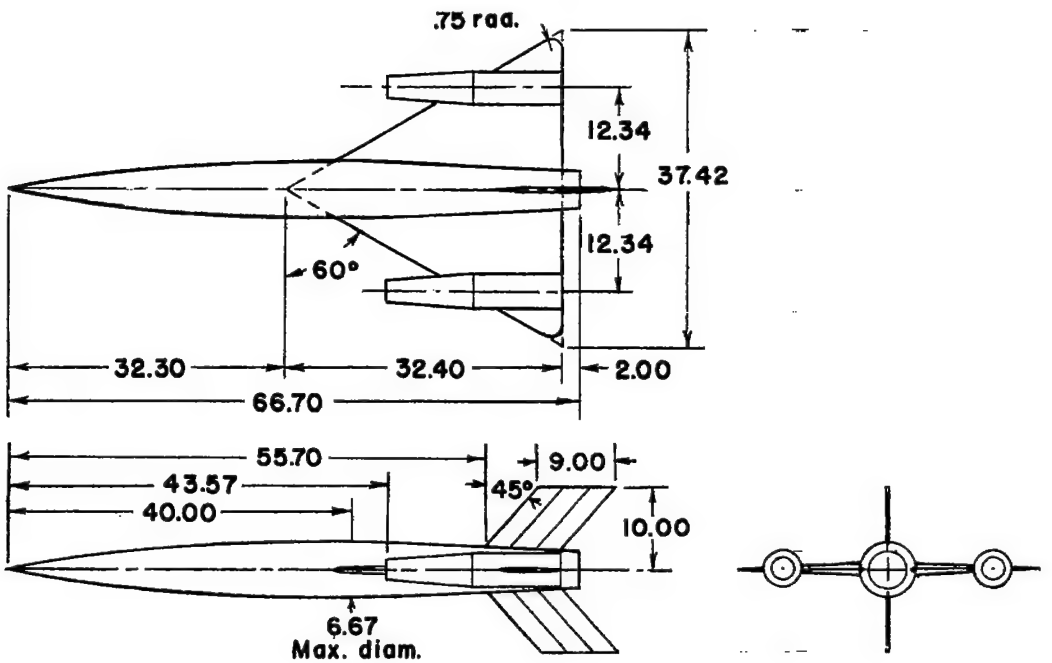

(b) Midwing configuration with symmetrical nacelles.

Figure 1.- Three-view drawings of test configurations. (All dimensions in inches.)

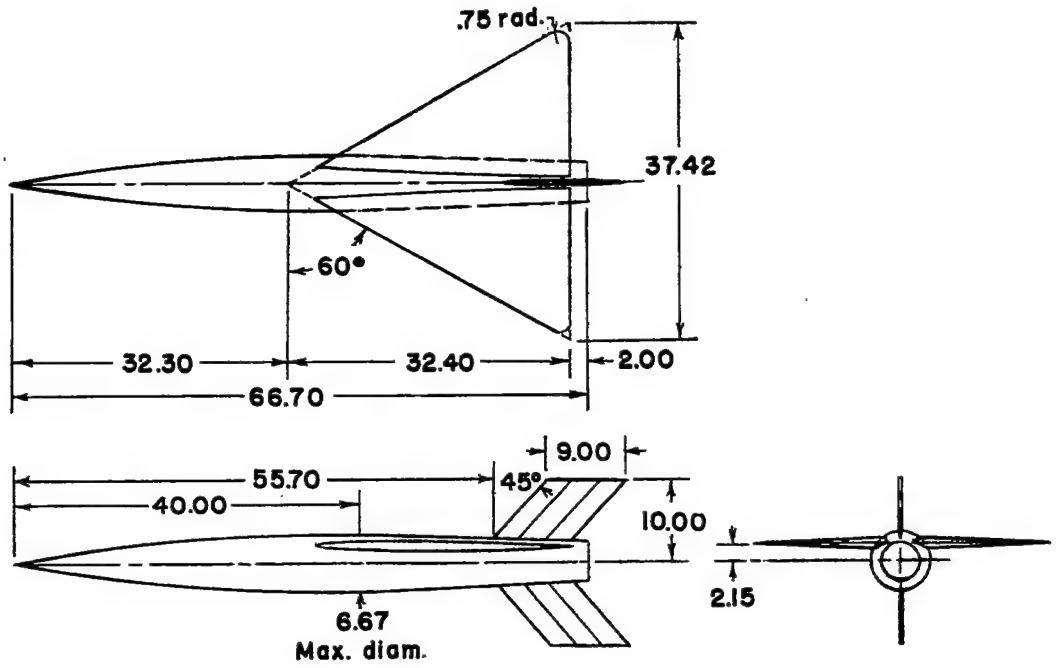

(c) High-wing configuration.

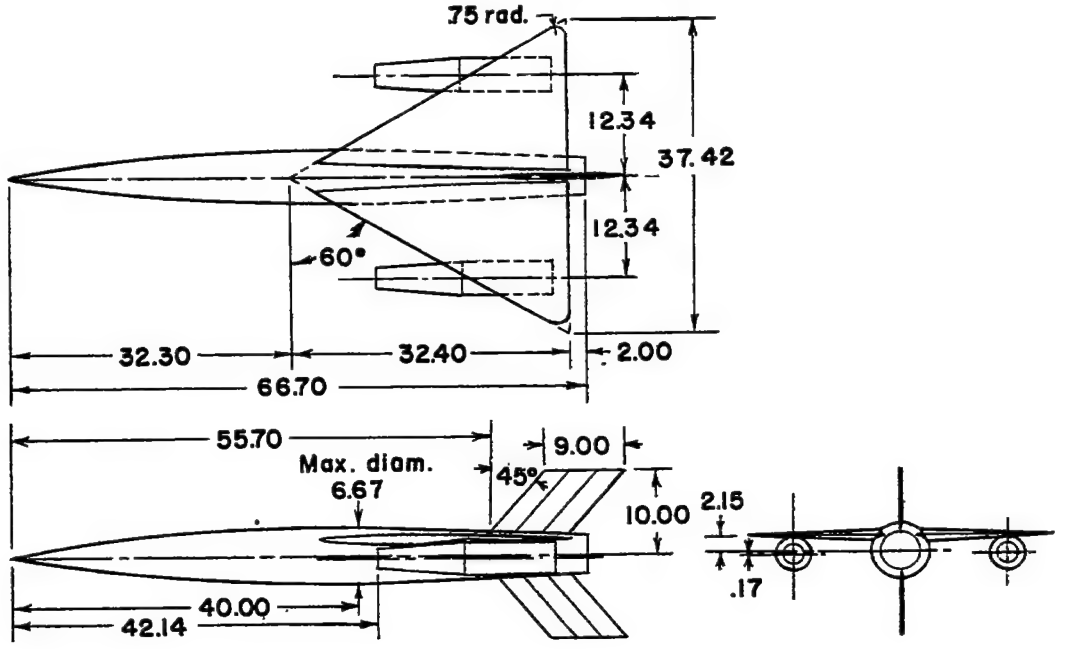

(d) High-wing configuration with underslung nacelles.

Figure 1.- Concluded.

[redacted]

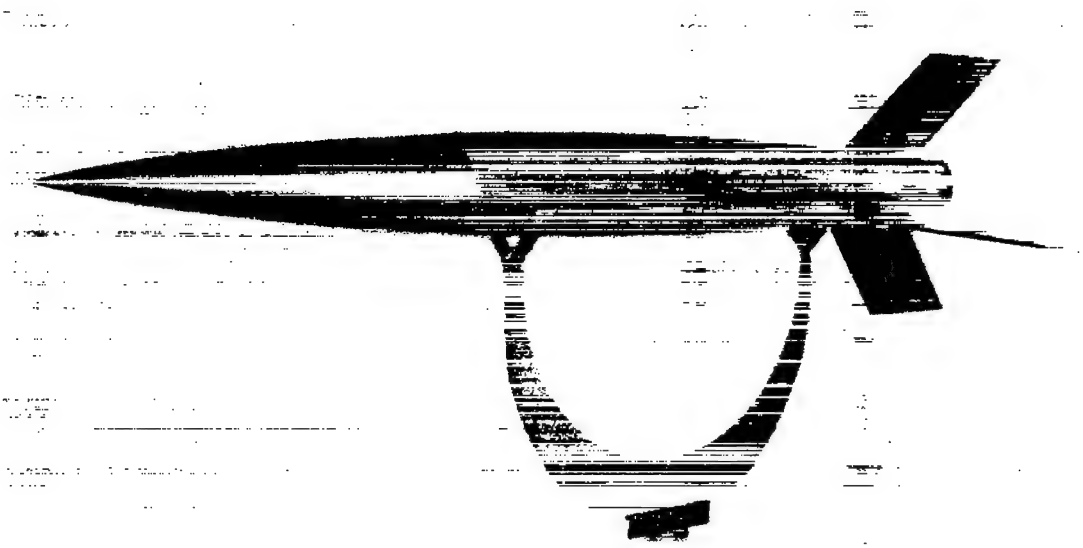

(a) Midwing configuration.

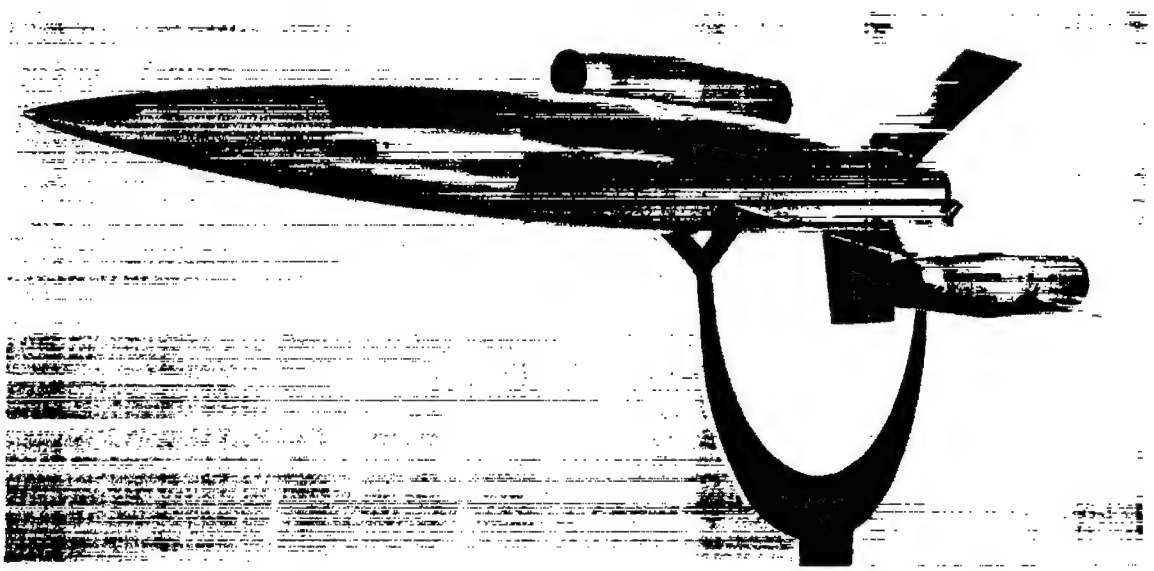

L-82065

(b) Midwing configuration with symmetrical nacelles.

Figure 2.- Photographs of models.

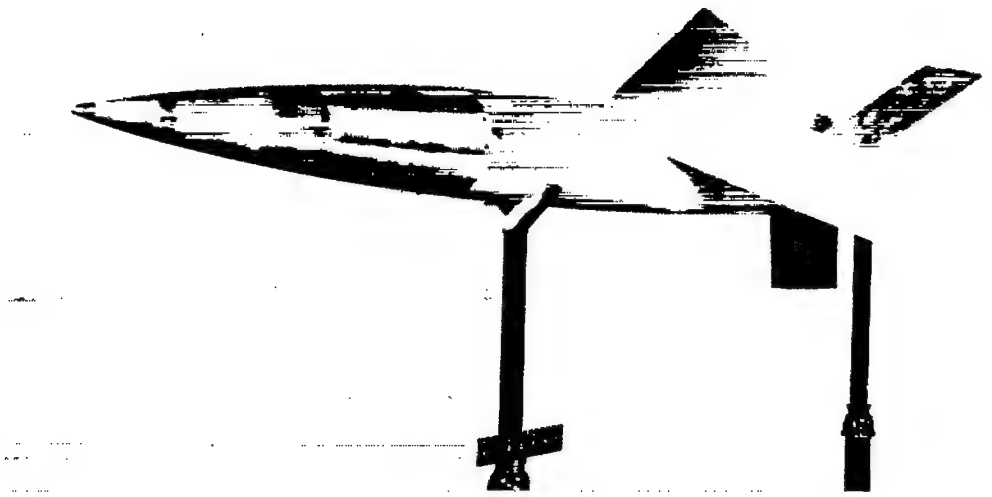

(c) High-wing configuration.

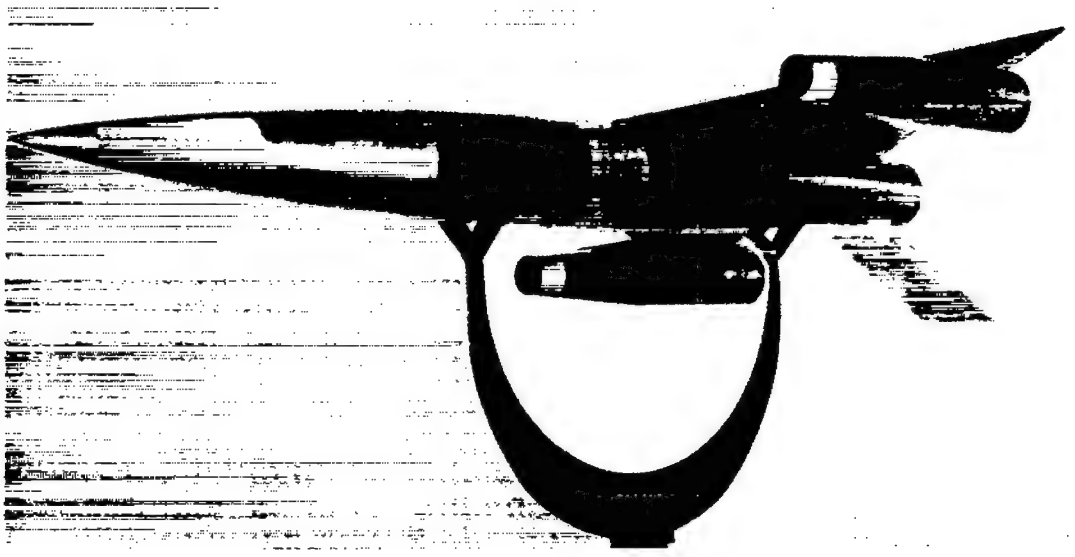

L-82066

(d) High-wing configuration with underslung nacelles.

Figure 2.- Continued.

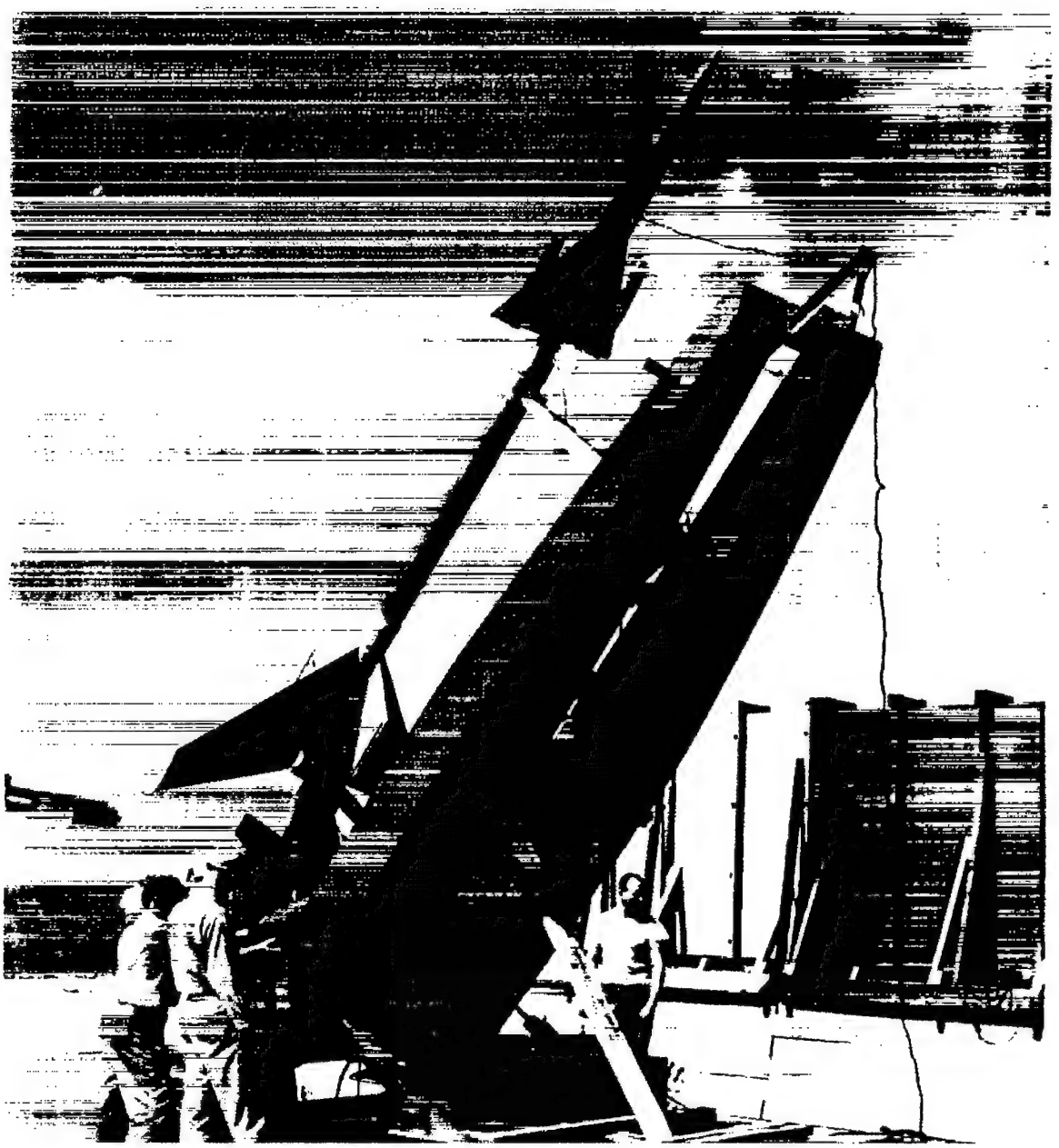

L-75534.1

(e) Model and booster on mobile launcher.

Figure 2.- Concluded.

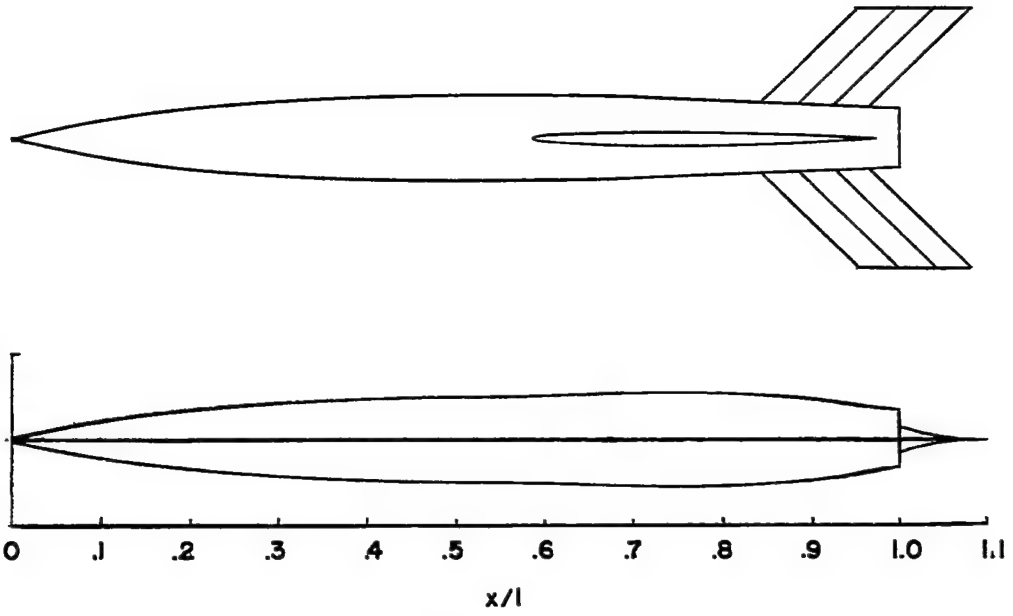

Equivalent body of revolution. Fineness ratio = 9.56.

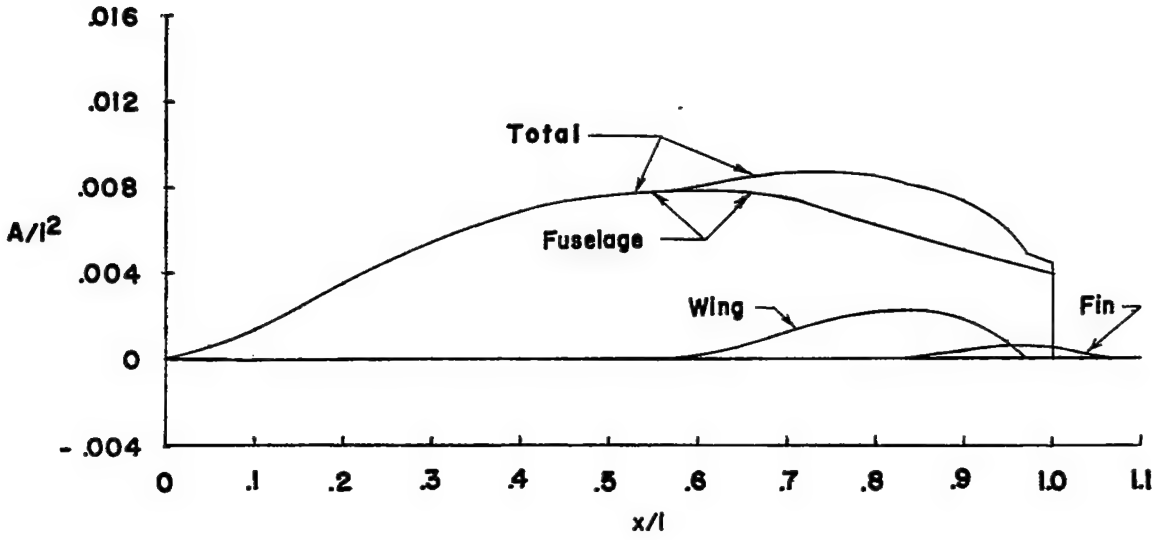

(a) Midwing configuration.

Figure 3.- Area distribution of test configurations.

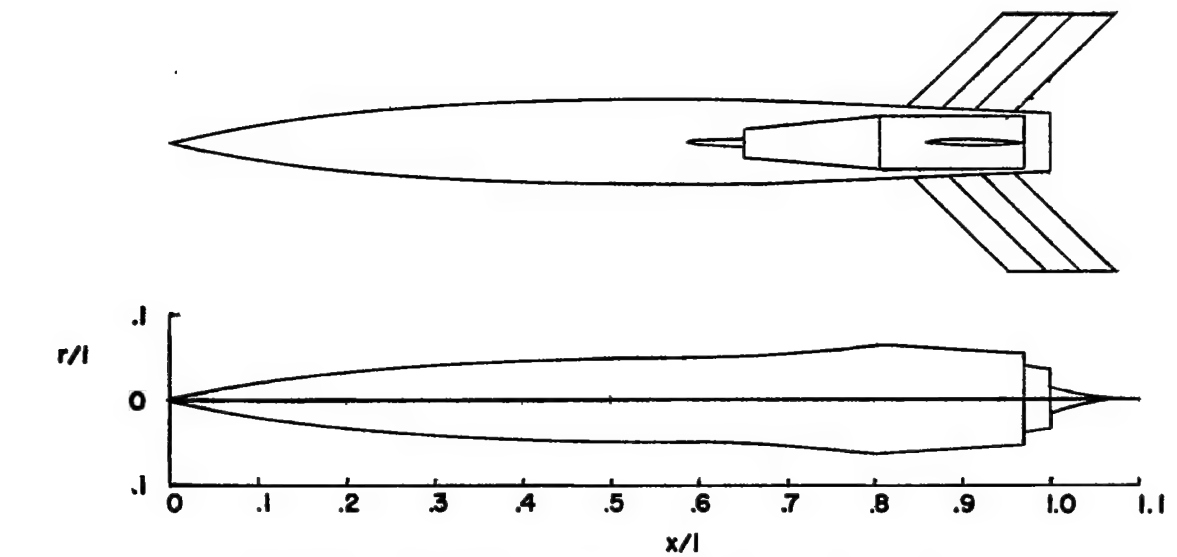

Equivalent body of revolution. Fineness ratio = 8.57.

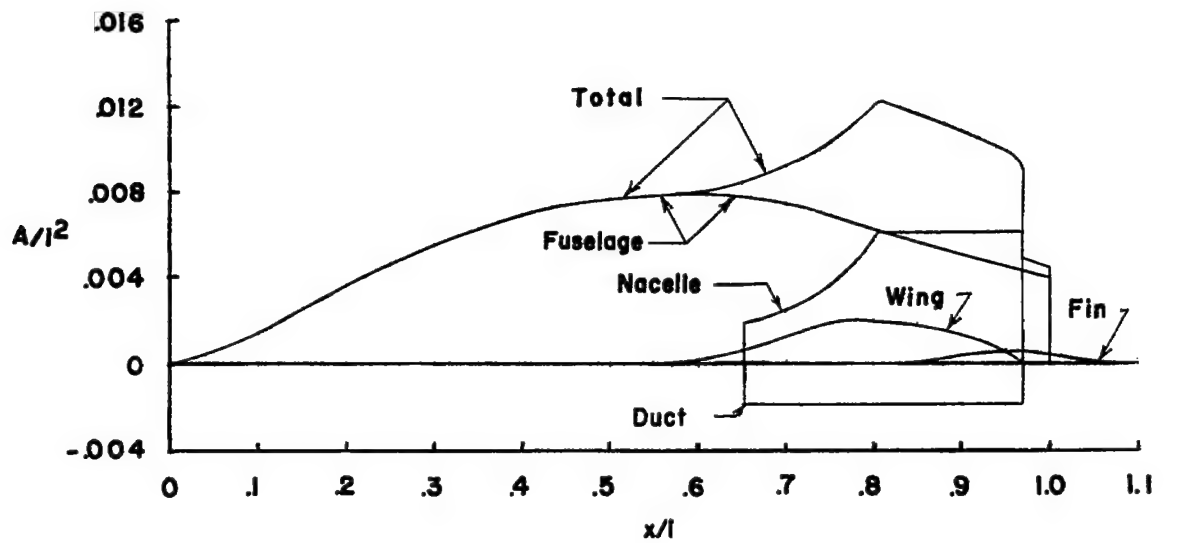

(b) Midwing configuration with symmetrical nacelles.

Figure 3.- Continued.

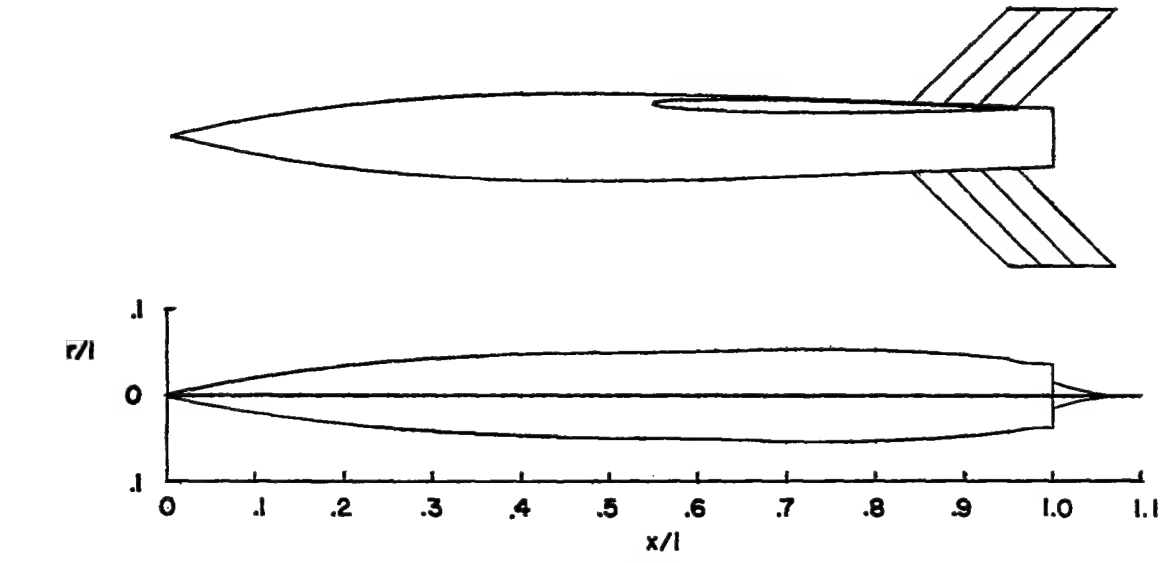

Equivalent body of revolution. Fineness ratio = 9.26.

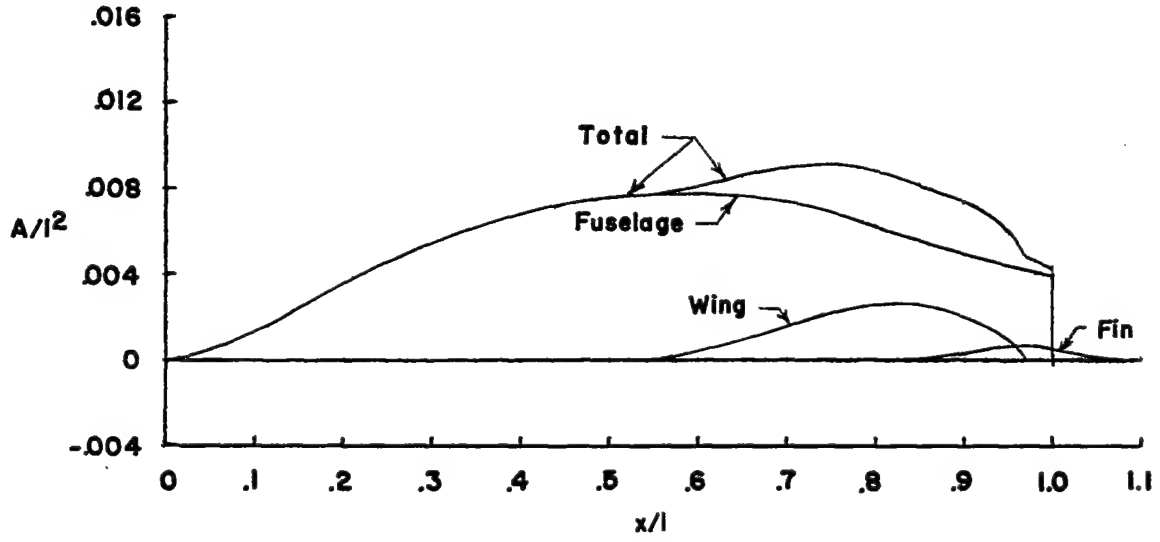

(c) High-wing configuration.

Figure 3.- Continued.

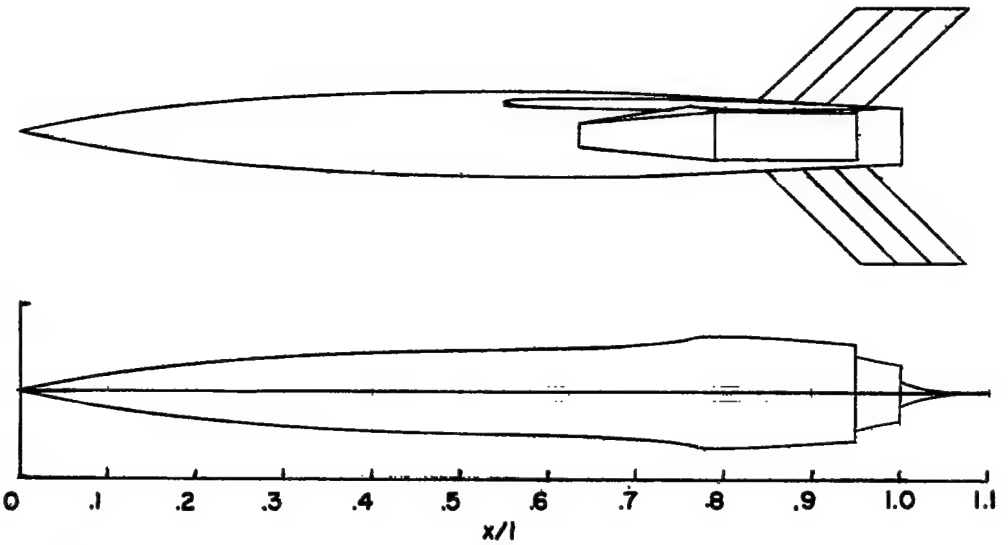

Equivalent body of revolution. Fineness ratio = 8.56.

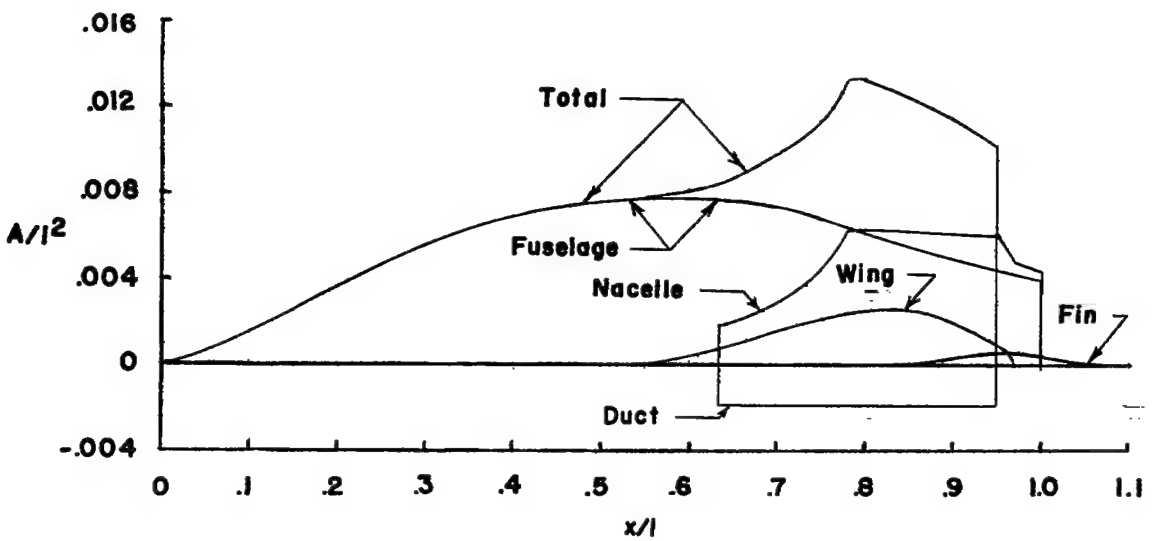

(d) High-wing configuration with underslung nacelles.

Figure 3.- Concluded.

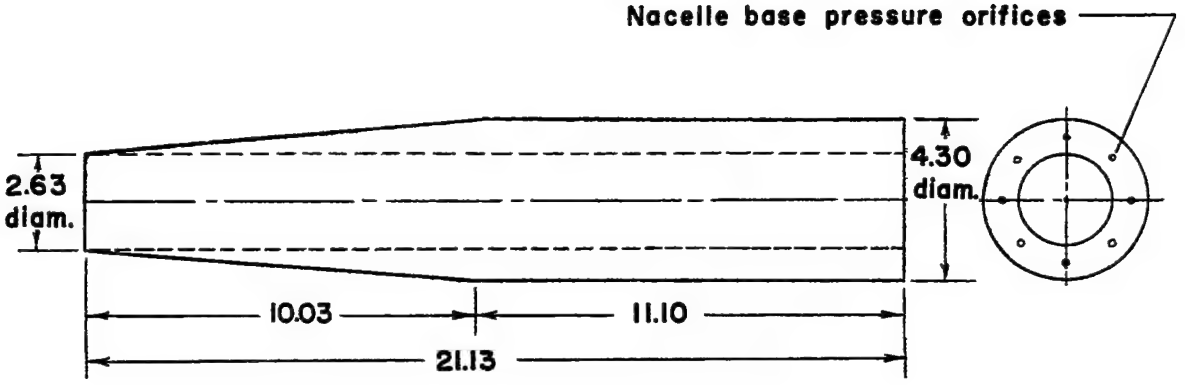

(a) Rocket-model nacelle.

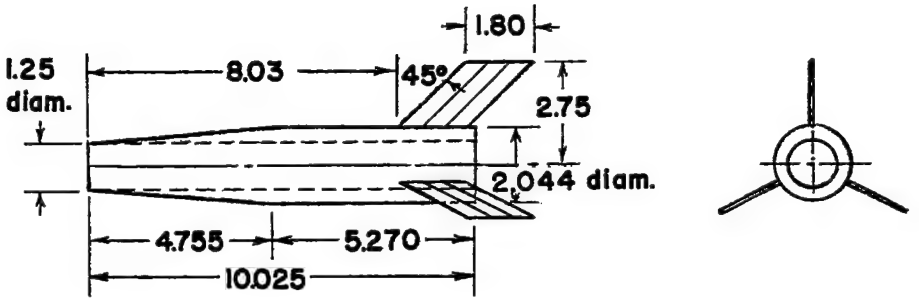

(b) Helium-gun nacelle.

Figure 4.- Drawings of test nacelles. (All dimensions in inches.)

L-82067

Figure 5.- Photograph of underslung nacelle showing wing-nacelle fairing.

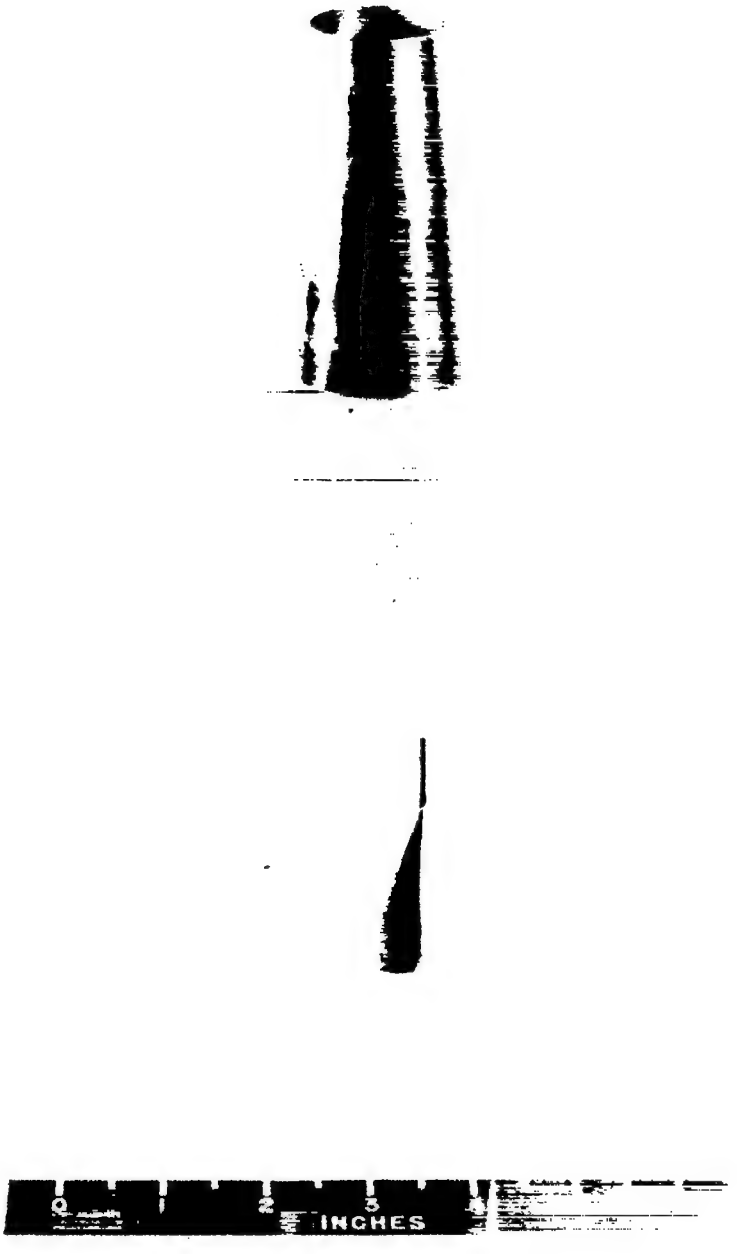

L-78554

Figure 6.- Helium-gun nacelle model.

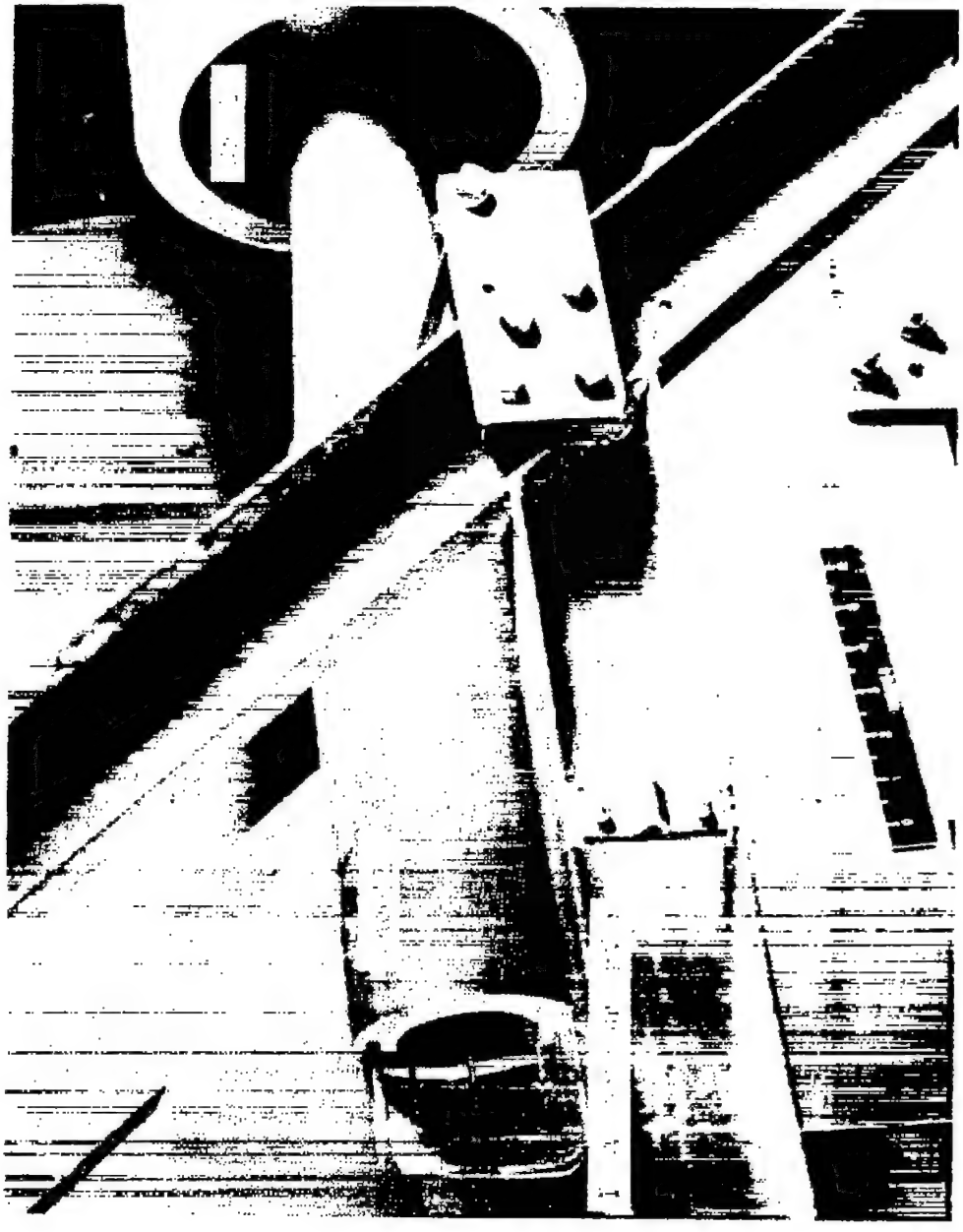

L-82068

Figure 7.- Nacelle installation in free jet.

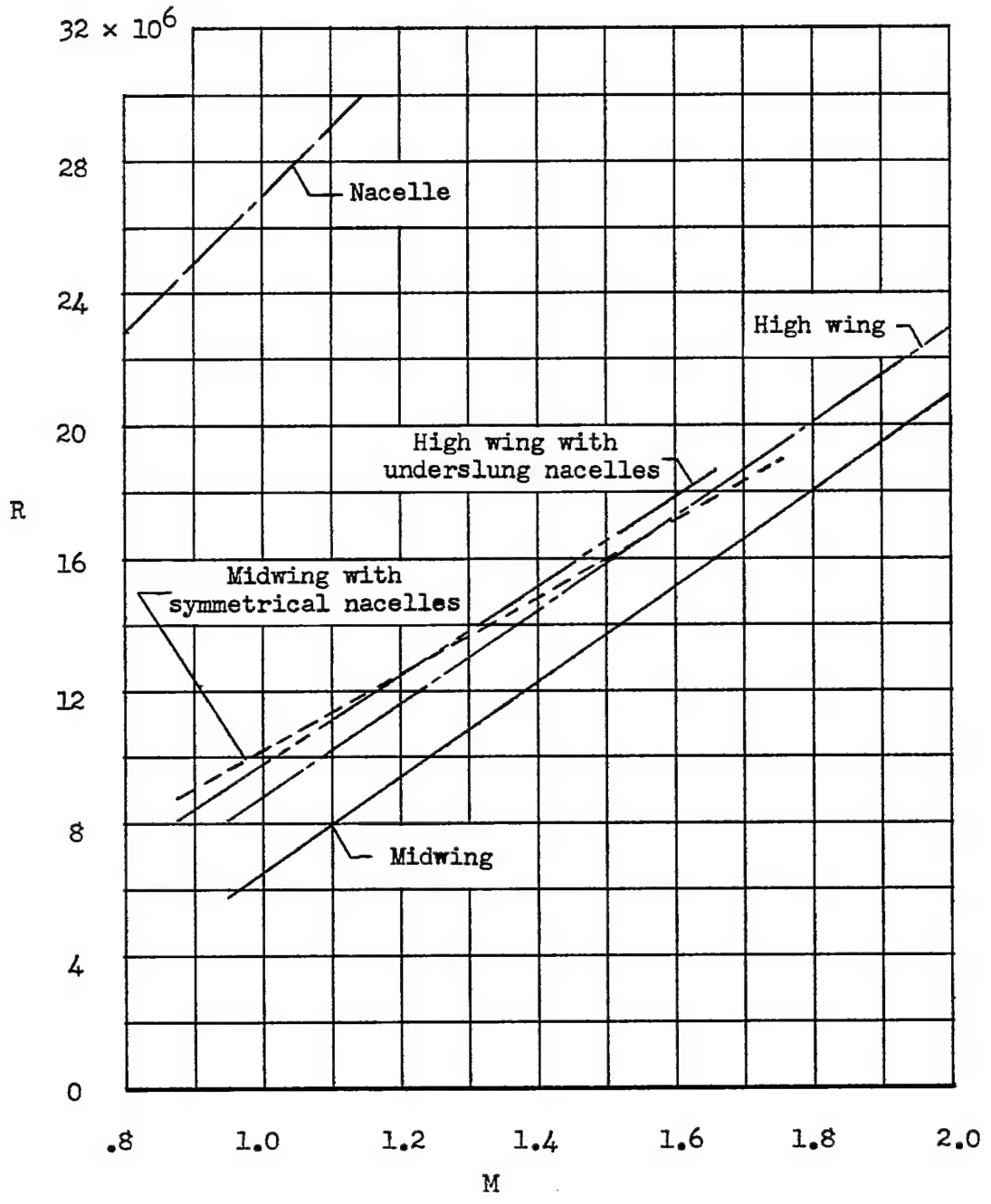

Figure 8.- Variation of Reynolds number, based on wing mean aerodynamic chord, with Mach number.

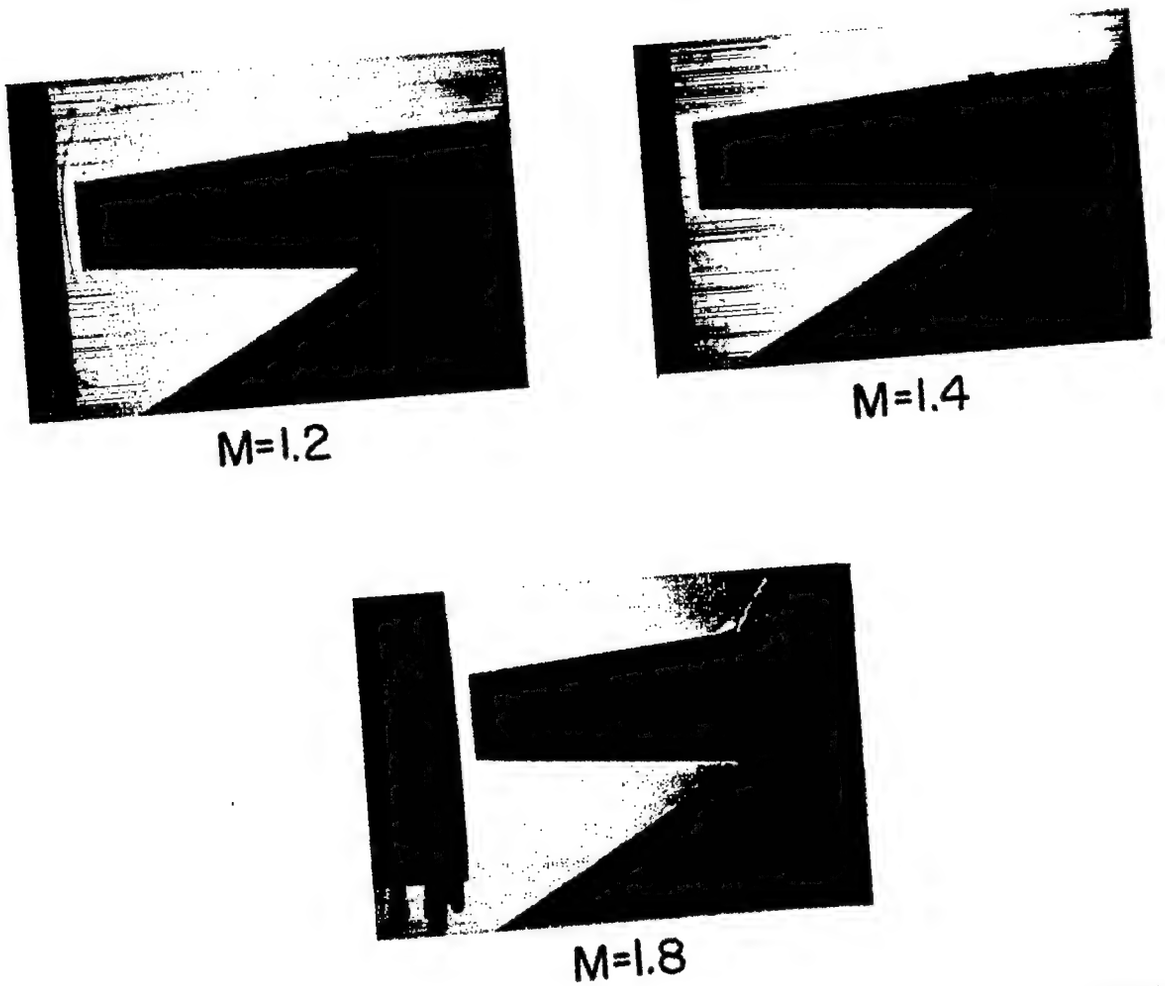

L-82069

Figure 9.- Shadowgraphs of flow at nacelle nose in free jet.

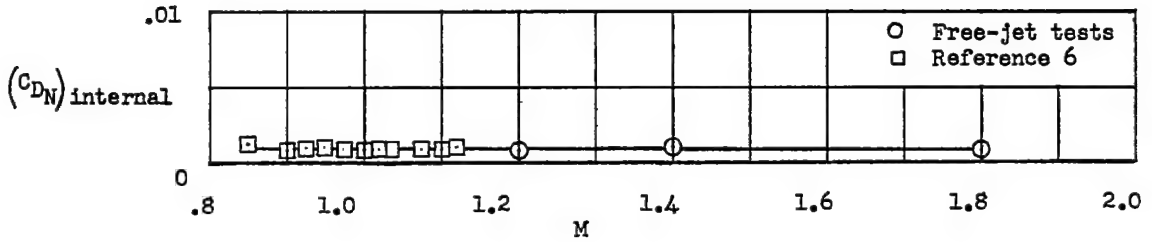

Figure 10.- Variation of nacelle internal drag coefficient based on wing area with Mach number for two nacelles.

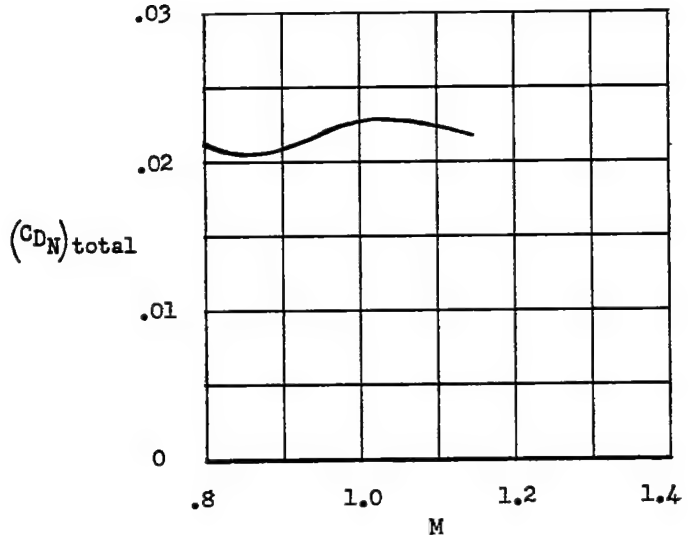

Figure 11.- Variation of total nacelle drag coefficient based on wing area with Mach number for two nacelles.

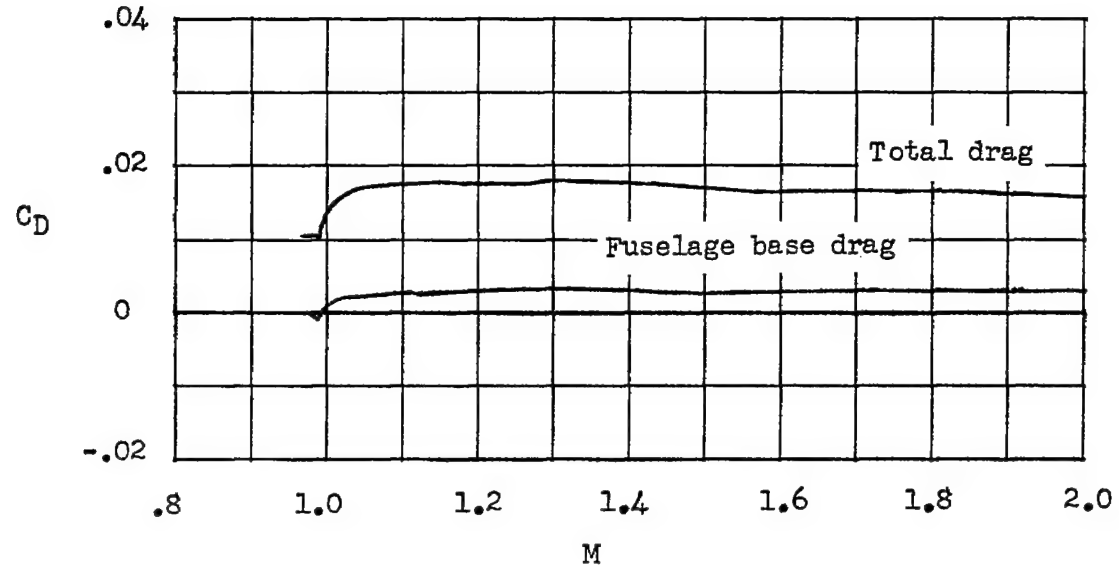

(a) Variation of drag coefficients with Mach number.

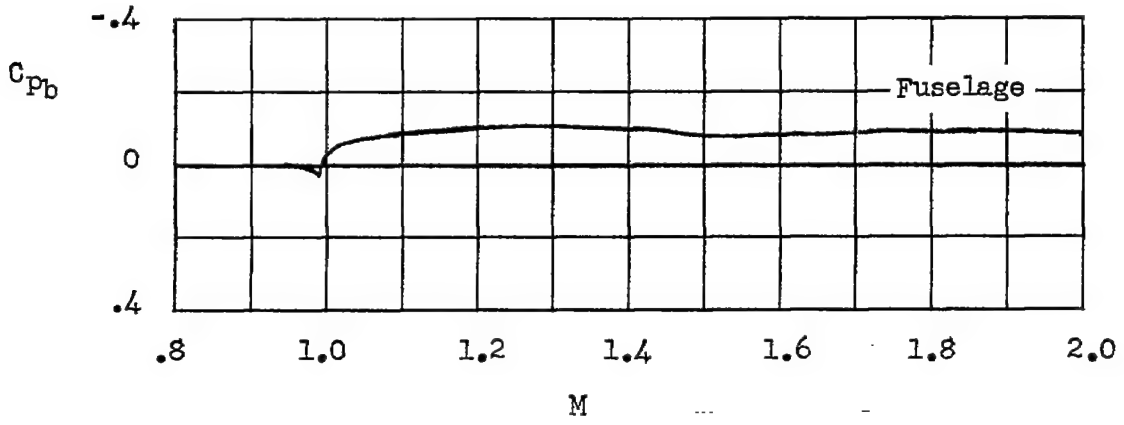

(b) Variation of base pressure coefficient with Mach number.

Figure 12.- Flight-test data for midwing configuration.

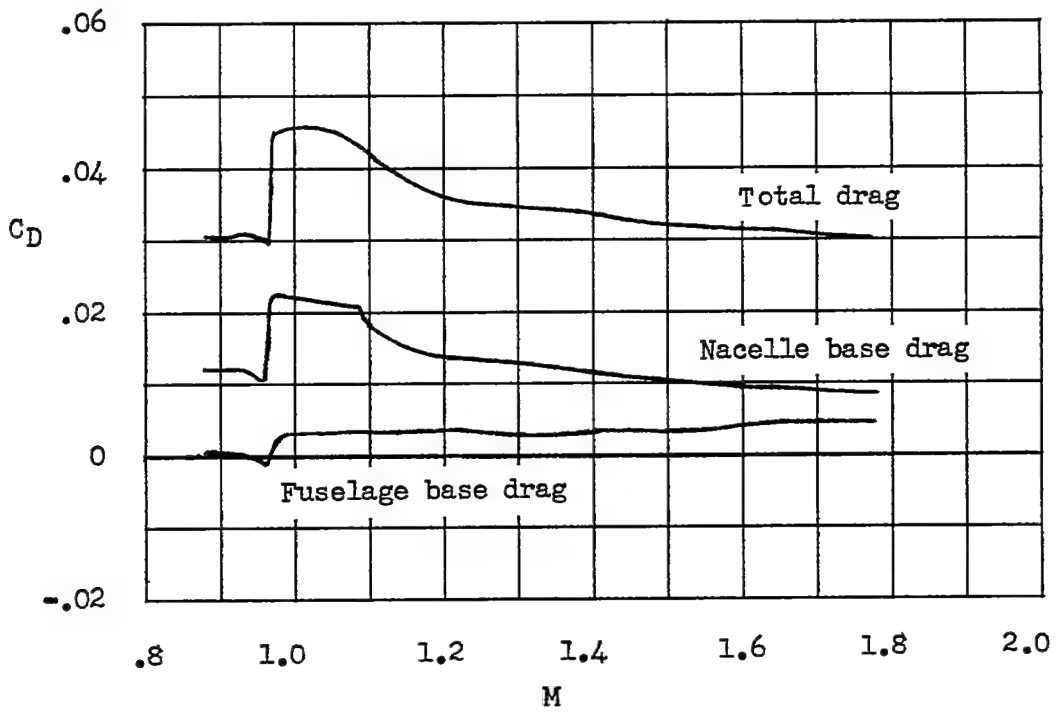

(a) Variation of drag coefficients with Mach number.

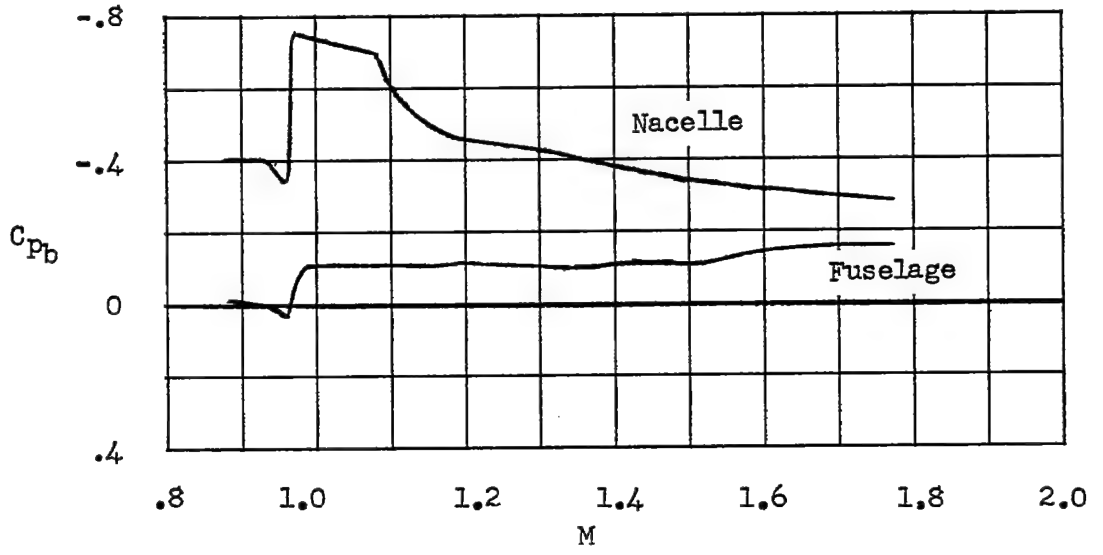

(b) Variation of base pressure coefficient with Mach number.

Figure 13.- Flight-test data for midwing configuration with symmetrical nacelles.

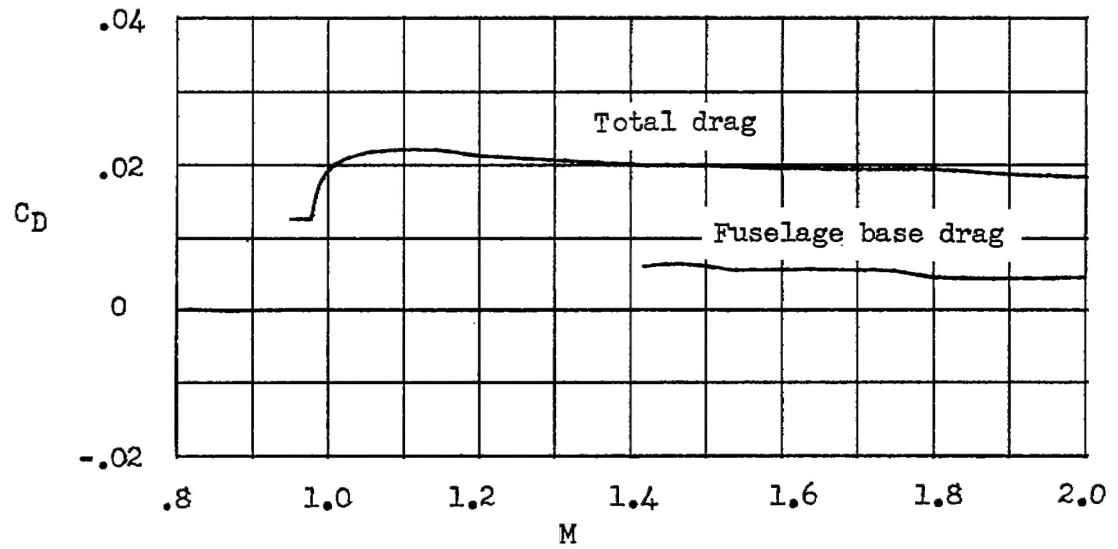

(a) Variation of drag coefficients with Mach number.

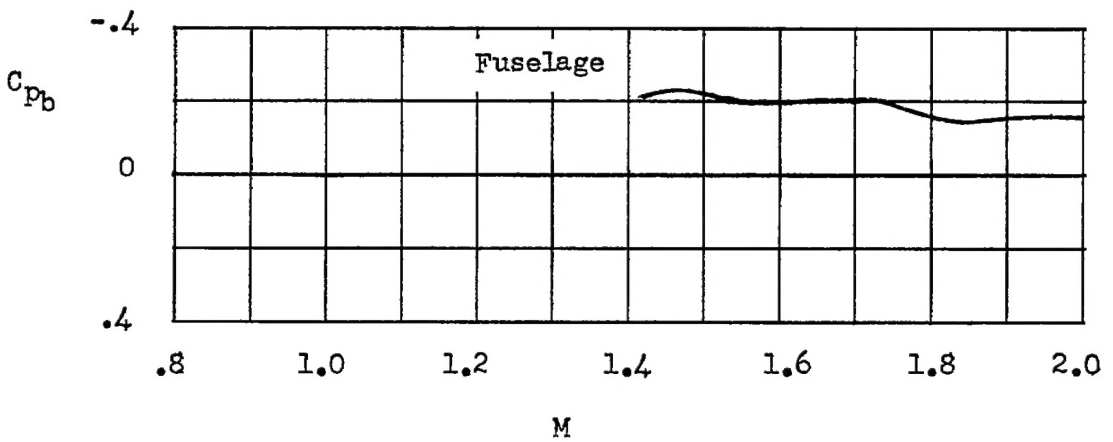

(b) Variation of base pressure coefficient with Mach number.

Figure 14.- Flight-test data for high-wing configuration.

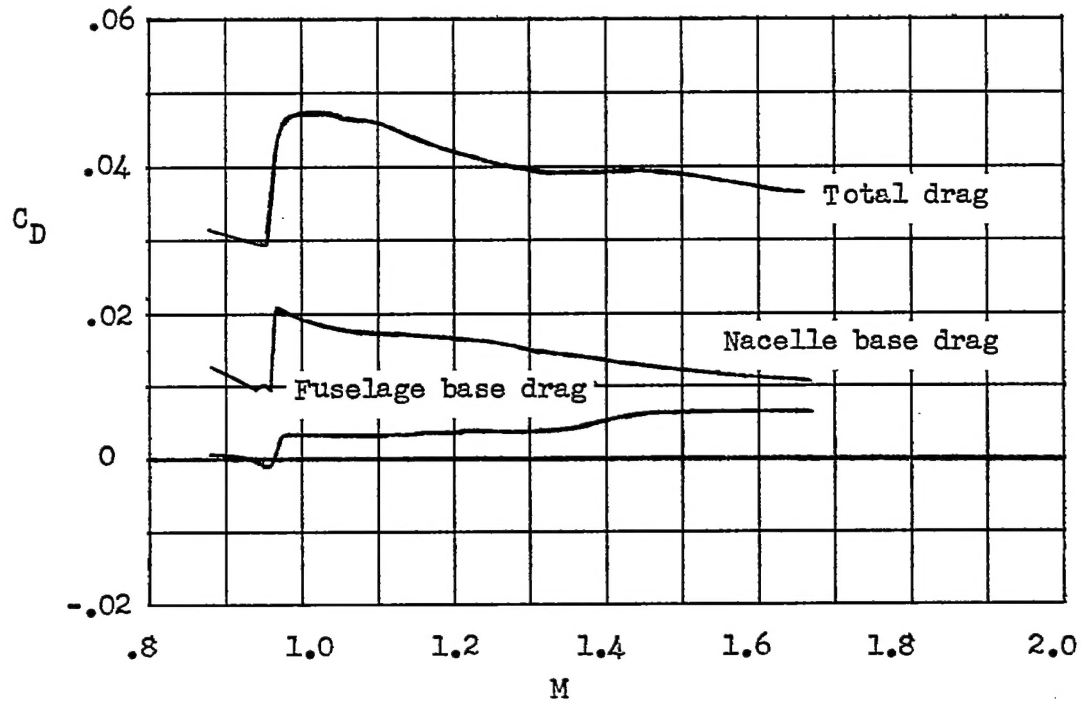

(a) Variation of drag coefficients with Mach number.

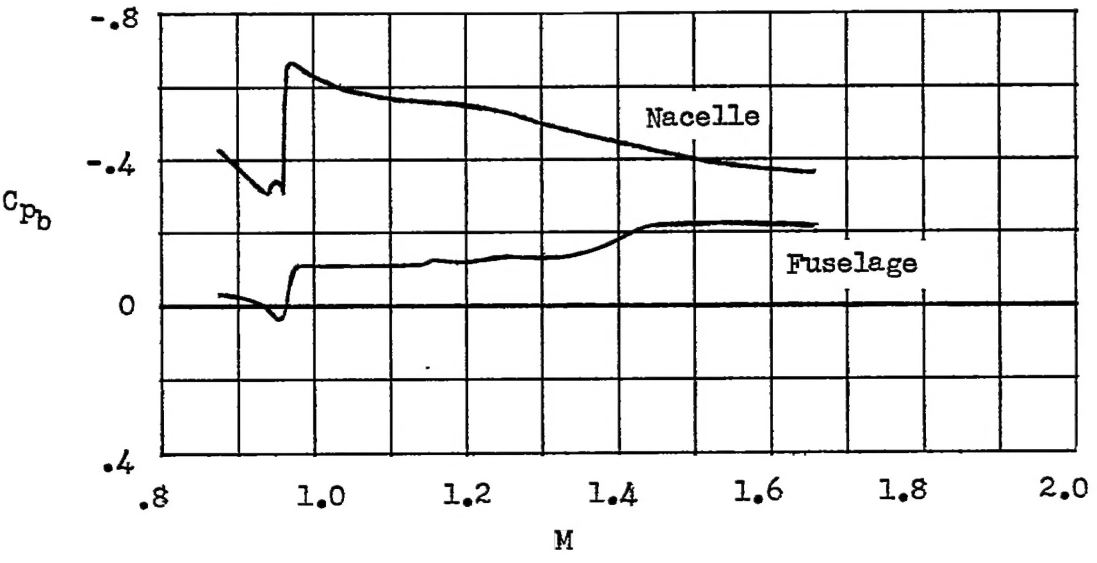

(b) Variation of base pressure coefficient with Mach number.

Figure 15.- Flight-test data for high-wing configuration with underslung nacelles.

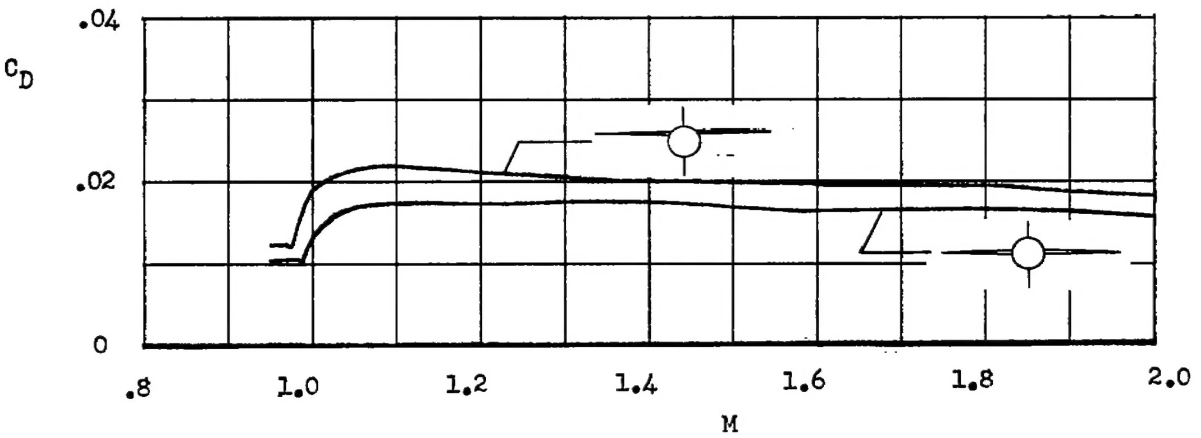

Figure 16.- Comparison of drag coefficients of high-wing and midwing configurations.

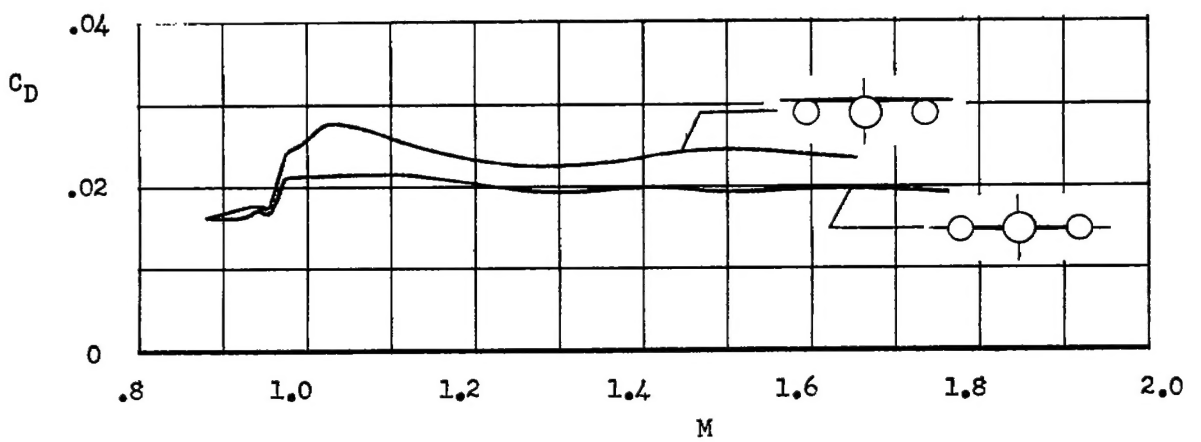

Figure 17.- Comparison of drag coefficients of high-wing and midwing configurations with nacelles. Nacelle base pressure adjusted to free-stream pressure.

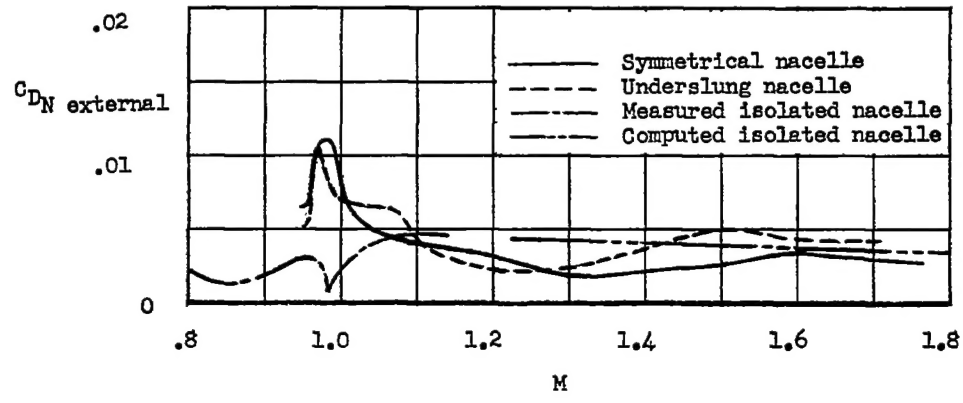

Figure 18.- Comparison of nacelle drag increment with drag coefficient of an isolated nacelle for two nacelles, based on wing area.

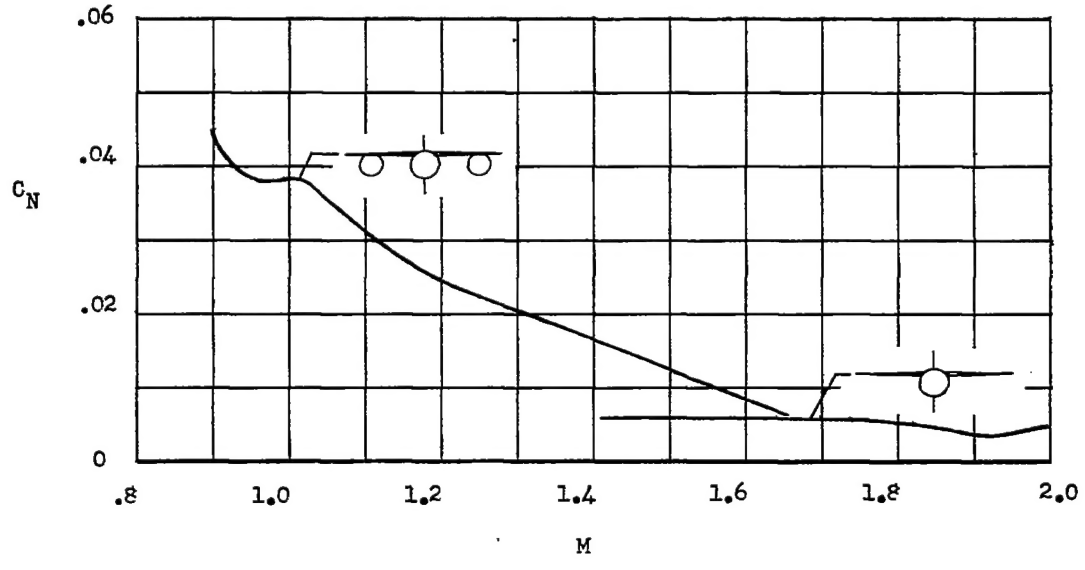

Figure 19.- Variation of normal force coefficient with Mach number for high-wing configurations.

NACA-Langley - 3-9-54 - 325